



CEBAF-TH-92-11

CEBAF

The Continuous Electron Beam Accelerator Facility
Theory Group Preprint Series

Additional copies are available from the authors.

The Southeastern Universities Research Association (SURA) operates the Continuous Electron Beam Accelerator Facility for the United States Department of Energy under contract DE-AC05-84ER40150

Forward peaking mechanism in proton Compton scattering

Simon Capstick

Continuous Electron Beam Accelerator Facility, Newport News, VA 23606

B. D. Keister

Department of Physics, Carnegie Mellon University, Pittsburgh, PA 15213

A simple explanation is given for the forward peaking observed in proton Compton scattering cross sections at photon energies above 800 MeV, in a nonrelativistic constituent quark model of the scattering process using intermediate resonances. This represents an alternate explanation to that using the standard vector-dominance model. Cross sections at these energies are calculated in a specific model, and the results compare favorably with the data, but the mechanism for forward peaking can be explained on rather general grounds.

DISCLAIMER

This report was prepared as an account of work sponsored by the United States government. Neither the United States nor the United States Department of Energy, nor any of their employees, makes any warranty, express or implied, or assumes any legal liability or responsibility for the accuracy, completeness, or usefulness of any information, apparatus, product, or process disclosed, or represents that its use would not infringe privately owned rights. Reference herein to any specific commercial product, process, or service by trade name, mark, manufacturer, or otherwise, does not necessarily constitute or imply its endorsement, recommendation, or favoring by the United States government or any agency thereof. The views and opinions of authors expressed herein do not necessarily state or reflect those of the United States government or any agency thereof.

I. INTRODUCTION

The high energy proton Compton scattering differential cross section, when plotted versus angle, exhibits strong forward peaking and a depletion in the backward direction. At 700 MeV, the forward peaking is already evident in the data from the Bonn group [1, 2] and the Tokyo group [3–5], though it is accompanied by a rise in the cross section at backward angles. As the photon energy increases from 700 MeV to 1000 MeV, the backward cross section decreases, and the forward peaking becomes more pronounced [1, 4, 6]. At even higher energies, the cross section data [2, 7–9] are very strongly forward peaked, with essentially an exponential falloff as a function of momentum transfer squared.

The shape of the cross section at the energies considered by the Bonn and Tokyo groups is typical [10] of the behavior of elastic hadron-hadron scattering cross sections at these energies. The rise in the cross section at backward angles is compared, in Ref. [1], to a similar rise in the mean value of the elastic π^+p and π^-p cross sections. The magnitude of the cross section is also comparable to that of this average, when multiplied by α_{QED}^2 . Comparisons have also been made [1, 2, 7–9] to the results of a vector dominance model (VDM), where the cross section for high-energy Compton scattering is related to that for the photoproduction of transversely polarized vector mesons. The Compton scattering cross section is written as

$$\frac{d\sigma(\gamma p \rightarrow \gamma p)}{dt} = \left\{ \sum_V \left(\alpha \left[\frac{4\pi}{f_V} \right]^2 \frac{d\sigma^{\text{tr}}(\gamma p \rightarrow V p)}{dt} \right)^{\frac{1}{2}} \right\}^2, \quad (1)$$

where the sum is over vector mesons $V = (\rho, \omega, \phi)$, f_V is the photon-vector meson coupling constant, and an upper limit has been formed by assuming constructive interference of the contributions from each meson. This procedure results in a roughly exponential falloff with $-t$ of the cross section away from the forward direction at 700 MeV and at higher energies. However the resulting value of f_ρ needed to fit the data at lower energies is smaller by a factor of two than the standard value [11] used in other processes.

The purpose of this paper is to provide a simple explanation for this forward

peaking of the cross section, and subsequent depletion at backward angles at higher energies, in terms of a nonrelativistic constituent quark model of Compton scattering. Our model is particularly suited to describing Compton scattering at these energies, where an intermediate-nucleon-resonance basis should be an efficient one. Three types of terms contribute to the Compton scattering amplitude in this picture; a ‘contact’ term with a two-photon interaction coupling directly to a quark line, a ‘direct’ term, corresponding to photoexcitation and deexcitation of baryon resonances in the s channel, and the ‘crossed’ version of the latter, corresponding to excitation and deexcitation of resonances in the u channel. We will show that at these energies, the contact term is forward peaked, and that the direct term for each resonance tends to enhance the forward amplitude, while tending to cancel in the backward direction. The crossed term is relatively small at higher energies due to large energy denominators.

This mechanism is demonstrated in a model of Compton scattering [12] using a nonrelativistic quark-photon interaction operator [13–15], and Isgur-Karl model [16–18] wavefunctions of the proton and intermediate resonances. The onset of strong forward peaking (and depletion at backward angles at higher energies) is evident in the shape of the differential cross sections which we calculate at 800, 950, 1230, and 1500 MeV, and their magnitudes compare roughly with the data from the Bonn and Tokyo groups [1–5].

This paper is organized as follows: the next section describes briefly our nonrelativistic constituent quark model for Compton scattering, with emphasis on the form of the amplitudes. There follows a description, in general terms, of the mechanism leading to forward peaking and depletion of the amplitude at backward angles. Differential cross sections are then calculated in the model of Ref. [12], illustrating this mechanism, and these calculations are compared with the data. In the last section, we discuss how the forward peaking of Compton amplitudes is an expected prediction of calculations employing intermediate baryon resonances.

II. COMPTON SCATTERING MODEL

Reference [12] provides extensive details for computing Compton scattering amplitudes in a nonrelativistic constituent quark model. We provide here the salient features most relevant to understanding the forward peaking mechanism. In particular, in this section, we avoid specific reference to actual model eigenstates, and discuss the origin of forward peaking on rather general grounds.

The Hamiltonian density for the interaction of photons with quark fields is [19]

$$\mathcal{H}(x) = \sum_i e_i I_{i\mu}(x) A^\mu(x), \quad (2)$$

where e_i is the charge of the i -th quark, $I_i^\mu(x) = \bar{q}_i(x)\gamma^\mu q_i(x)$ is the quark current, and $A^\mu(x)$ is the photon field. In a nonrelativistic valence quark model, the effective Hamiltonian has both one-photon and two-photon terms:

$$H_{\text{photon}} = H_\gamma + H_{\gamma\gamma}. \quad (3)$$

The one-photon contribution is, for real transverse photons:

$$H_\gamma = - \sum_i e_i \mathbf{I}_i(\mathbf{r}_i) \cdot \mathbf{A}(\mathbf{r}_i), \quad (4)$$

and the two-photon contact interaction is

$$H_{\gamma\gamma} = \sum_i \frac{e_i^2}{2m_i} [\mathbf{A}(\mathbf{r}_i)]^2 q_i^\dagger(\mathbf{r}_i) q_i(\mathbf{r}_i). \quad (5)$$

The Compton amplitude can then be written as follows:

$$T = \langle f | H_{\gamma\gamma} | i \rangle + \sum_n \frac{\langle f | H_\gamma | n \rangle \langle n | H_\gamma | i \rangle}{E_i + \omega - E_n} + \sum_n \frac{\langle f | H_\gamma | n \rangle \langle n | H_\gamma | i \rangle}{E_i - \omega' - E_n}, \quad (6)$$

where ω and ω' are the initial and final photon energies, E_i is the initial baryon energy and E_n is the energy of the intermediate hadronic state.

In our constituent (valence) quark model, we assume that the Hilbert space consists entirely of the set of baryons generated from that model. If the γN system has an overall momentum \mathbf{P} , and the initial and final photon momenta are \mathbf{k} and \mathbf{k}' , respectively, then the Compton amplitude is

$$T = e^2 \sum_{\lambda'\lambda} \frac{1}{\sqrt{2\omega'}\sqrt{2\omega}} \epsilon'^*_{\lambda'} T_{\lambda'\lambda} \epsilon_\lambda, \quad (7)$$

where

$$\begin{aligned} T_{\lambda'\lambda} = & \sum_i \langle N; \mathbf{P} - \mathbf{k}' | \frac{e_i^2}{2e^2 m_i} q_i^\dagger(0) q_i(0) \delta_{\lambda'\lambda} | N; \mathbf{P} - \mathbf{k} \rangle \\ & + \sum_n \frac{\langle N; \mathbf{P} - \mathbf{k}' | I_{-\lambda'}^\dagger(0) | X_n; \mathbf{P} \rangle \langle X_n; \mathbf{P} | I_\lambda(0) | N; \mathbf{P} - \mathbf{k} \rangle}{\omega + \omega_{M_N}(\mathbf{P} - \mathbf{k}) - \omega_{M_n}(\mathbf{P})} \\ & + \sum_n \frac{\langle N; \mathbf{P} - \mathbf{k}' | I_{-\lambda'}^\dagger(0) | X_n; \mathbf{P} - \mathbf{k} - \mathbf{k}' \rangle \langle X_n; \mathbf{P} - \mathbf{k} - \mathbf{k}' | I_\lambda(0) | N; \mathbf{P} - \mathbf{k} \rangle}{-\omega' + \omega_{M_N}(\mathbf{P} - \mathbf{k}) - \omega_{M_n}(\mathbf{P} - \mathbf{k} - \mathbf{k}')}, \end{aligned} \quad (8)$$

and

$$\omega_m(\mathbf{p}) \equiv \sqrt{m^2 + \mathbf{p}^2}. \quad (9)$$

The symbol X_n stands for any baryon in the spectrum. The hadronic currents $I_\lambda(0)$ are represented in a constituent quark model as a sum of individual quark currents, as in Eq. 4.

III. FORWARD PEAKING MECHANISM

We now examine the role of each of the three contributions to Eq. 8 with regard to the forward peaking behavior. We consider explicitly the forward and backward directions, because all momenta in those cases lie on a single axis, and this simplifies greatly the expression for the Compton amplitude. In the forward direction, there is coherent enhancement of the superposed contributions, while in the backward direction, there is considerable cancellation. Because each resonant contribution involves only a complex phase in going from zero to 180 degrees, we expect a smooth transition of the overall amplitude between forward and backward directions.

The contact term consists of a positive definite quantity multiplying a polarization product ($\epsilon'^* \cdot \epsilon$). This product by itself gives rise to an unpolarized (Thomson) cross section proportional to $(1 + \cos^2 \theta)$. However, the matrix element between initial and final nucleon states gives rise to a body form factor

which falls off with momentum transfer. These two features combine to give a partial Compton amplitude which is forward peaked and backward suppressed.

The direct term involves a sum over all baryon resonances permitted by selection rules. In the forward direction ($\mathbf{k}' = \mathbf{k}$), the Compton amplitude must be diagonal in nucleon and photon spins:

$$\begin{aligned} T_{\lambda\lambda}^{\text{direct}}(\mathbf{k}' = \mathbf{k}) &= \sum_n \frac{\langle N; -\mathbf{k}\mu | I_{-\lambda}^\dagger(0) | X_n; \mathbf{0}\nu \rangle \langle X_n; \mathbf{0}\nu | I_\lambda(0) | N; -\mathbf{k}\mu \rangle}{\sqrt{s} - M_n + i\Gamma_n/2} \\ &= \sum_n \frac{|\langle X_n; \mathbf{0}\nu | I_\lambda(0) | N; -\mathbf{k}\mu \rangle|^2}{\sqrt{s} - M_n + i\Gamma_n/2} \\ &= \sum_n \frac{|A_\nu^N(X_n)|^2}{\sqrt{s} - M_n + i\Gamma_n/2}, \end{aligned} \quad (10)$$

where $\nu = \lambda + \mu$, $A_\nu^N(X_n)$ is the helicity- ν photoexcitation amplitude for the resonance X_n , and we have included the width Γ_n of the intermediate resonances in the energy denominators.

Equation 10 shows that the direct contribution to the forward amplitude from any resonance X_n has a real part which has the sign of $\sqrt{s} - M_n$, and a negative imaginary part. For masses in the resonance sum which are less than \sqrt{s} , their forward direct contributions will add constructively to the forward-peaked contact term. For masses above \sqrt{s} , their contributions will subtract from the real part and add to the imaginary part. Since there is an unlimited spectrum above \sqrt{s} , one might expect that these contributions would easily cancel those contributions below \sqrt{s} , if not completely dominate the Compton amplitude. However, this does not happen, and the amplitude is not strongly affected by the addition of these higher mass states. This is demonstrated in our explicit model calculation, but can also be understood on general grounds; the energy denominators for high-mass intermediate resonances damp their contributions, and the matrix elements for high-mass excitations rapidly become small for increasing resonance energy and fixed photon frequency. Theoretically, the latter is to be expected (and is confirmed in the discussion below for a specific quark model) because the photon eventually does not provide the necessary phase matching between the nucleon ground state and an excited state containing many nodes in

its spatial wave function. Experimentally [20], few of the high-mass resonances established in the πN partial-wave analyses are resolved in the photoproduction analyses. For baryons with mass in the vicinity of \sqrt{s} , the real parts of their energy denominators are small, but the imaginary parts add coherently.

In the backward direction, the spins are all the same as they are for the forward direction, but the photon and nucleon final momenta are now reversed. The amplitude is

$$\begin{aligned} T_{\lambda\lambda}^{\text{direct}}(\mathbf{k}' = -\mathbf{k}) &= \sum_n \frac{\langle N; +\mathbf{k}\mu | I_{-\lambda}^\dagger(0) | X_n; \mathbf{0}\nu \rangle \langle X_n; \mathbf{0}\nu | I_\lambda(0) | N; -\mathbf{k}\mu \rangle}{\sqrt{s} - M_n + i\Gamma_n/2} \\ &= \sum_n \frac{\langle X_n; \mathbf{0}\nu | I_\lambda(0) | N; +\mathbf{k}\mu \rangle^* \langle X_n; \mathbf{0}\nu | I_\lambda(0) | N; -\mathbf{k}\mu \rangle}{\sqrt{s} - M_n + i\Gamma_n/2} \\ &= - \sum_n P_n \frac{|A_\nu^N(X_n)|^2}{\sqrt{s} - M_n + i\Gamma_n/2}, \end{aligned} \quad (11)$$

where we have used parity to replace $\langle X_n; \mathbf{0}\nu | I_\lambda(0) | N; \mathbf{k}\mu \rangle$ with $-P_n A_\nu^{N*}(X_n)$, and P_n is the parity of the resonance X_n . If we evaluate this sum at, say, $\sqrt{s}=1800$ MeV ($E_{\text{lab}}=1250$ MeV), *i.e.*, at sufficiently high energy that many resonances play a role, the contributions from the band of low-lying negative parity resonances in the spectrum will cancel against those from the ground and excited state positive parity states below this energy. This cancellation is not exact, as it depends on the number of states of a given parity and the size of their photocouplings, but it is not an enhanced coherent sum as is the case in the forward direction, and the contribution in the backward direction is therefore greatly reduced with respect to the forward direction. Those amplitudes with opposite forward *vs.* backward phase essentially have a complex phase at intermediate angles, so we expect a smooth transition from forward to backward angles.

As the photon energy is increased, more and more resonances add coherently to the forward angle amplitude, and cancel each other with mixed phase at backward angles. The backward-angle cross section will be roughly constant, while the forward-angle cross section will continue to rise with increasing photon energy. Indeed this behavior is necessitated by the optical theorem: above 1000 MeV the total γp cross section saturates to a constant, and this in turn yields

a forward scattering amplitude whose imaginary part is dominant, and equal to $\omega\sigma_{\text{tot}}/4\pi$. The result is a lower bound for the forward Compton differential cross section which is proportional to ω^2 .

A similar analysis can be made for the crossed term. In the forward direction,

$$T_{\lambda\lambda}^{\text{crossed}}(\mathbf{k}' = \mathbf{k}) = \sum_n \frac{|A_\nu^N(X_n)|^2}{\sqrt{s} - 2\omega - \sqrt{M_n^2 + 4\mathbf{k}^2} + i\Gamma_n/2}, \quad (12)$$

and at backward angles,

$$T_{\lambda\lambda}^{\text{crossed}}(\mathbf{k}' = -\mathbf{k}) = \sum_n -P_n \frac{|A_\nu^N(X_n)|^2}{\sqrt{s} - 2\omega - \sqrt{M_n^2 + 4\mathbf{k}^2} + i\Gamma_n/2}; \quad (13)$$

Considering the *numerators* of these expressions, the same analysis of forward peaking and backward suppression applies as it does for the direct term. However, at the energies considered here, the energy denominators for the crossed terms are large, and their overall effect is negligible when compared to the direct sums or the contact term.

IV. DIFFERENTIAL CROSS SECTIONS

We now demonstrate the forward peaking mechanism specifically for the non-relativistic quark model used in Ref. [12]. We also make comparisons of calculated differential cross sections to data at a set of energies where the onset of forward peaking is clearly seen experimentally.

The Compton scattering amplitude is calculated in Ref. [12] with the formulae of Eqs. 7 and 8, using a nonrelativistic reduction of the current $I_{i\mu}(x)$, which is written in terms of the usual quark-spin-flip and orbit-flip (convection) operators. The current matrix elements are evaluated using nonrelativistic quark model wavefunctions of the Isgur-Karl model. These wavefunctions are based on a harmonic oscillator basis set, with configuration mixing induced by the color-hyperfine interaction. The formally infinite set of intermediate states in Compton scattering is truncated at the mixed states in the $N = 2$ band in the oscillator, which are positive-parity excited Nucleon and Δ states; this set of thirty states exhausts, with a few exceptions, all of the well known states below about 2000

MeV. It also includes states present in the model which, for reasons well understood [13], have not been discovered in photoproduction or pion-production experiments.

In Fig. 1 we have plotted the partial cross sections at 1230 MeV lab photon energy (E_γ) resulting from the contact term, the direct sum, and the crossed sum, as well as the complete cross section from Eq. 8, formed with all thirty intermediate states. In order to address the issue of the convergence of our calculation, we have also plotted the complete cross section using only those (thirteen) intermediate states which lie *below* $\sqrt{s} = 1785$ MeV. Both the contact term and the direct sum show the expected forward peaking, and are small at backward angles. The crossed sum is relatively small at all angles. The forward cross section is thus dominated by a contact term and a direct sum which add roughly in phase.

The effect of adding in the states in our model *above* \sqrt{s} is shown by the difference between the two complete cross section curves in Fig. 1. The minor difference at forward angles is an indicator that the photocouplings to these states are quite small. In the Isgur-Karl model, these photocouplings have been studied by Koniuk and Isgur [13]. Table III from Ref. [13] expresses the photocouplings as functions of K/α , where $K = |\mathbf{k}|$, and α is oscillator size parameter. For any given photon momentum K/α , the constant coefficients multiplying these expressions will eventually suppress the photocouplings of highly excited states, if one goes high enough in the oscillator spectrum. The individual resonance contributions to our sums are proportional to the square of these photocouplings, which (for $E_\gamma = 1230$ MeV or $K = 646$ MeV) are generally smaller for the states above $\sqrt{s} = 1785$ MeV. There is some reduction of the real part of the direct sum of Eq. 11 from these states with negative $\sqrt{s} - M_n$, and an increase of the imaginary part; the net change to the magnitude of the complete sum is small. This photon energy was chosen as an upper limit to the range of energies at which our calculation can be argued roughly to have converged; the addition of states neglected in the model of Ref. [12] will affect the cross section, but because of the increase of the energy denominators and decrease of the photocoupling amplitudes, we expect the final shape to retain the strong forward peaking and

backward angle depletion shown in Fig. 1.

Data in the energy range at which this forward peaking becomes evident have been taken by groups at Bonn [1, 2], Tokyo [3–6] and MIT [21]. Figures 2, 3, 4 and 5 compare the differential cross section calculated with the model of Ref. [12] and these data. In all cases the calculated cross section is shown along with the partial cross sections from the contact term, the direct sum, and the crossed sum.

At 800 MeV the calculated cross section is slightly higher at forward angles than at backward angles, with a dip at roughly 90 degrees, which agrees well with the shape of the data. The cross section is dominated by the direct sum which, when added to the forward-peaked contact term, shows this slight forward peaking. As the energy is increased from 800 to 950 MeV ($\sqrt{s} = 1543$ to 1632 MeV) the direct sum increases at forward angles, as more states contribute to the sum with positive energy denominators, and decreases at backward angles, as more of the negative parity states pick up positive energy denominators. When added to the contact term the result is a more strongly forward peaked amplitude which no longer increases at backward angles. Once again the calculation is in rough agreement with both the shape and magnitude of the data.

As the energy is increased to 1230 MeV ($\sqrt{s} = 1785$ MeV) and 1500 MeV ($\sqrt{s} = 1922$ MeV) the forward peaking becomes more pronounced, due to the coherent phase of the individual resonance contributions to the direct sum once \sqrt{s} is above the mass of those resonances with the largest electromagnetic couplings. The cancellation at backward angles is much more effective once sizeable numbers of states with positive and negative parities lie below \sqrt{s} . Although the data at these energies are limited to a range of angles between 30 and 90 degrees, they also exhibit small cross sections at larger angles and a trend towards stronger peaking at forward angles.

The calculation overshoots the forward cross section at these higher energies. A discrepancy of the magnitude shown is not surprising, given the sensitivity of the overall magnitude of the cross section to the size of the resonance electromagnetic couplings, which enter to the fourth power. Furthermore, although these couplings generally decrease as the mass of the resonances increase, the majority of the intermediate states which have been neglected lie above these \sqrt{s} values

and make negative contributions to real part of the direct sum at forward angles. A more complete sum may decrease the direct sum but should not significantly affect the cancellation at backward angles. These neglected states are less important at lower \sqrt{s} values because of their relatively large energy denominators.

V. DISCUSSION

We have shown that the forward peaking behavior of proton Compton scattering in the GeV region can be explained in the context of the nonrelativistic quark model. While the actual calculations which were compared to data indeed made use of this model, the basis for forward peaking can be understood in more general terms. Equation 6 characterizes any theory in which the Hilbert space is saturated by baryon resonances, and need not refer to any specific quark model. The two-photon Hamiltonian $H_{\gamma\gamma}$ must have a specific structure at low momentum transfer in order to be consistent with Low's theorem [22], and would generally be expected to have a body form factor commensurate with the spatial structure of the proton, as evidenced by the so-called recoil contribution to the proton polarizability, which is proportional to the mean square charge radius [23]. The arguments leading to Eqs. 10 and 12 are geometric in nature, and do not depend upon specific details of a quark model. Thus, we expect on a qualitative basis that any model based upon intermediate baryon resonances should predict a Compton amplitude which is forward peaked, and more sharply so with increasing energy.

VI. ACKNOWLEDGEMENTS

We wish to thank Dr. Bernhard Mecking and Prof. Reinhard Schumacher for their questions which prompted us to undertake this study. This work was supported in part by U.S. National Science Foundation under Grant No. PHY-9023586 (BDK) and the U.S. Department of Energy under Contract No. DE-AC05-84ER40150 (SC).

REFERENCES

- [1] M. Jung, J. Kattein, H. Kück, P. Leu, K.-D. de Marné, R. Wedemeyer and N. Wermes, *Zeit. Phys. C10*, 197 (1981).
- [2] J. Duda, F.-W. Höfner, M. Jung, R. Kleissler, H. Kück, P. Leu, K.-D. de Marné, B. Munk, W. Vogl and R. Wedemeyer, *Zeit. Phys. C17*, 319 (1983).
- [3] K. Toshioka, M. Chiba, S. Kato, K. Sugano, K. Ukai, T. Shimomura, T. Shinohara, M. Daigo, Y. Hemmi, R. Kikuchi, M. Minowa, K. Miyake, T. Nakamura, A. Noda, M. Ono, Y. Suzuki, M. Yoshioka and Y. Hoshi, *Nucl. Phys. B141*, 364 (1978).
- [4] T. Ishii, K. Egawa, S. Kato, T. Miyachi, K. Sugano, K. Toshioka, K. Ukai, M. Chiba, K. Joh, T. Shinohara, Y. Yoribayashi and Y. Wada, *Nucl. Phys. B165*, 189 (1980).
- [5] Y. Wada, K. Egawa, A. Imanishi, T. Ishii, S. Kato, K. Ukai, F. Naito, H. Nara, T. Noguchi and K. Takahashi, *Nucl. Phys. B247*, 313 (1984).
- [6] T. Ishii, K. Egawa, A. Imanishi, S. Kato, Y. Takeuchi, K. Ukai, M. Yoshioka, T. Noguchi, T. Ohmori, N. Shimura K. Takahashi and Y. Wada, *Nucl. Phys. B254*, 458 (1985).
- [7] G. Buschhorn, L. Criegee, G. Franke, P. Heide, R. Kotthaus, G. Poelz, U. Timm, G. Vogel, K. Wegener, H. Werner and W. Zimmermann, *Phys. Lett. 33B*, 241 (1970); *Phys. Lett. 37B*, 207 (1971).
- [8] R.L. Anderson, D. Gustavson, J. Johnson, I. Overman, D. Ritson, B.H. Wilk, R. Talman, J.K. Walker and D. Worcester, *Phys. Rev. Lett. 25*, 1218 (1970).
- [9] A.M. Boyarski, D.H. Coward, S. Ecklund, B. Richter, D. Sherden, R. Siemann and C. Sinclair, *Phys. Rev. Lett. 26*, 1600 (1971).
- [10] H. Harari, *Ann. Phys. 63*, 432 (1971); Proceedings of the 1971 Symposium on Electron Photon Interactions, Cornell, p. 304 (1972).
- [11] T.H. Bauer, R.D. Spital, D.R. Yennie and F.M. Pipkin, *Rev. Mod. Phys. 50*, 261 (1978).
- [12] S. Capstick and B.D. Keister, CEBAF preprint CEBAF-PR-91-22, to appear in *Phys. Rev. D* (1992).
- [13] R. Koniuk and N. Isgur, *Phys. Rev. D21*, 1868 (1980).
- [14] C.P. Forsyth and R.E. Cutkosky, *Phys. Rev. Lett. 46*, 576 (1981); *Zeit. Phys. C18*, 219 (1983).
- [15] R. Sartor and Fl. Stancu, *Phys. Rev. D31*, 128 (1985); *Phys. Rev. D33*, 727 (1986).
- [16] N. Isgur and G. Karl, *Phys. Lett. 72B*, 109 (1977); *Phys. Lett. 74B*, 353 (1978); *Phys. Rev. D18*, 4187 (1978).
- [17] N. Isgur and G. Karl, *Phys. Rev. D19*, 2653 (1979).
- [18] N. Isgur, G. Karl and R. Koniuk, *Phys. Rev. Lett. 41*, 1269 (1978); *Phys. Rev. D25*, 2394 (1982).
- [19] We take $\hbar = c = 1$ and use Heaviside-Lorentz units, whereby $\alpha_{\text{QED}} = e^2/4\pi \approx 1/137$.
- [20] J.J. Hernández *et al.* (the Particle Data Group), *Phys. Lett. 239B*, 1 (1990).
- [21] M. Deutsch, K.J. Cleetus, L. Golub, D.F. Jacobs, P. Kijewski, E. Loh, G. Marini, P.M. Patel, D. Potter, R. Stiening and K. Tsipis, *Phys. Rev. D8*, 3828 (1973).
- [22] F. E. Low, *Phys. Rev. 96*, 1428 (1954); M. Gell-Mann and M. L. Goldberger, *Phys. Rev. 96*, 1433 (1954).
- [23] V. A. Petrun'kin, *Fiz. Elem. Chastits At. Yadra 12*, 692 (1981) [*Sov. J. Part. Nucl. 12*, 278 (1981)].

FIGURES

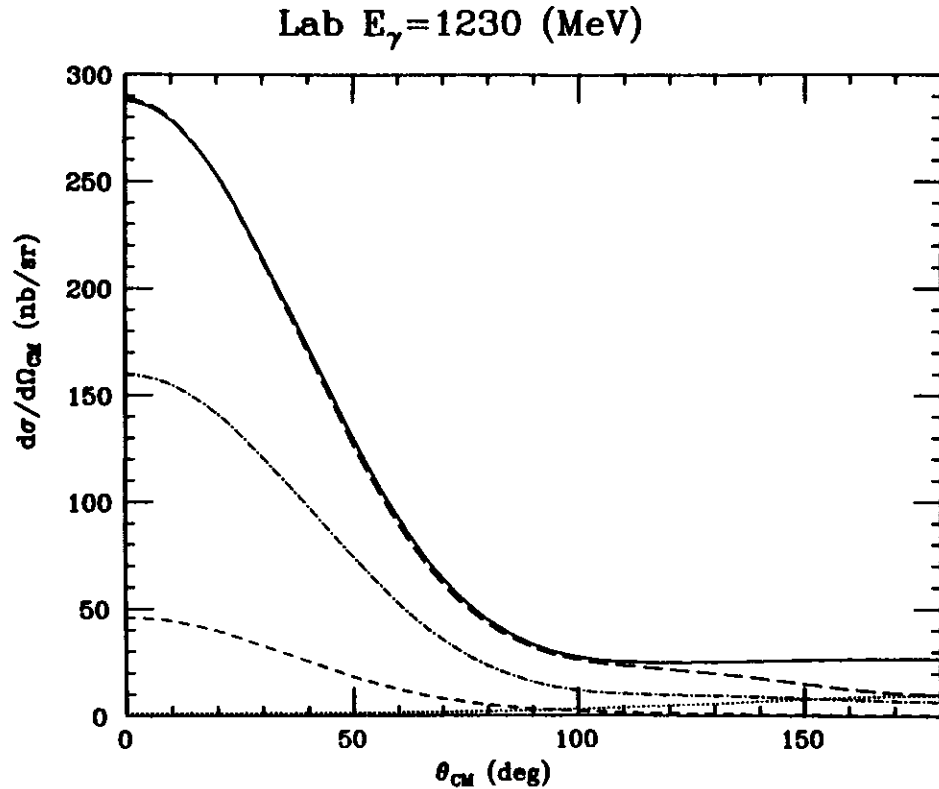


FIG. 1. Calculated center-of-momentum (CM) frame differential cross section for Compton scattering at $E_\gamma = 1230$ MeV with contributions from all states considered in Ref. [12]. The dashed line is the partial cross section from the contact term, the dashed-dotted from the direct sum, the dotted from the crossed sum, and the solid line is the complete cross section. The long-dashed line is the complete cross section with contributions from states with $M_n < \sqrt{s}$.

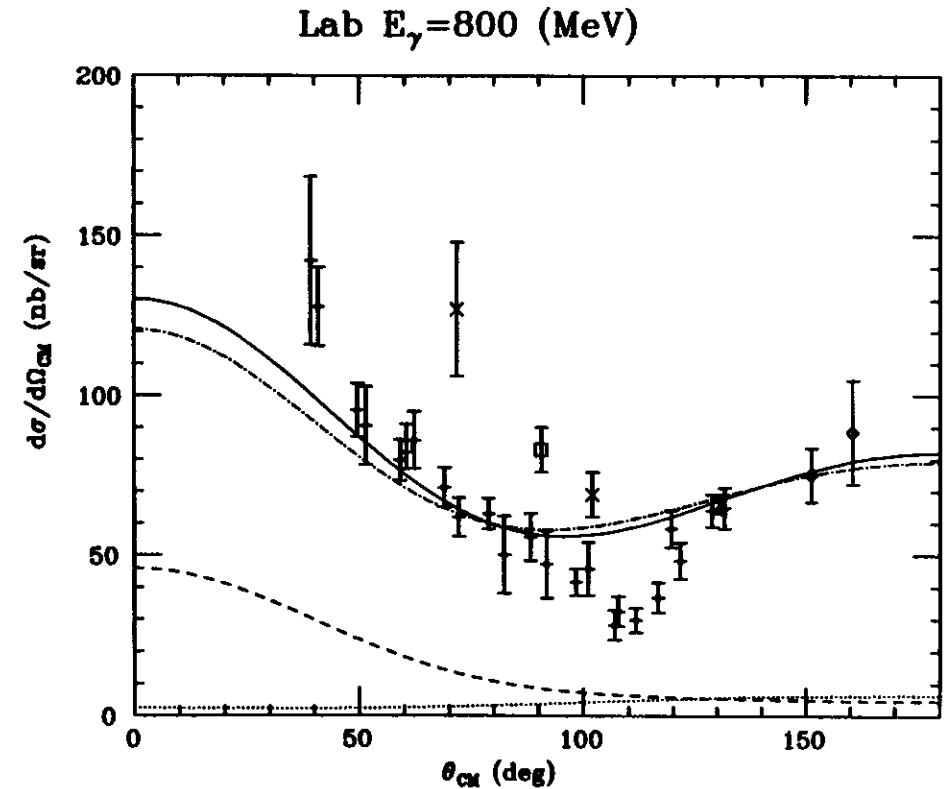


FIG. 2. CM frame differential cross section at $E_\gamma = 800$ MeV with contributions from all states considered in Ref. [12]. The dashed line is the partial cross section from the contact term, the dashed-dotted from the direct sum, the dotted from the crossed sum, and the solid line is the complete cross section. Data are from Ref. [1] (crosses), Ref. [3] (boxes), Refs. [4, 6] (X's), and Ref. [5] (diamonds).

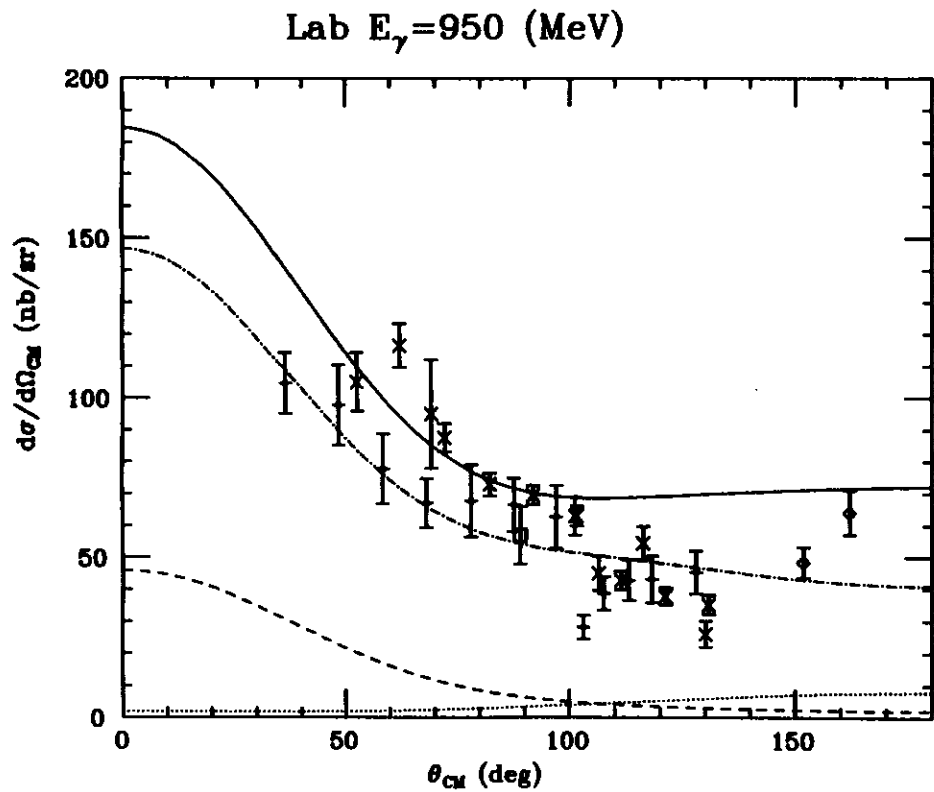


FIG. 3. CM frame differential cross section at $E_\gamma = 950$ MeV. Legend as in Fig. 2.

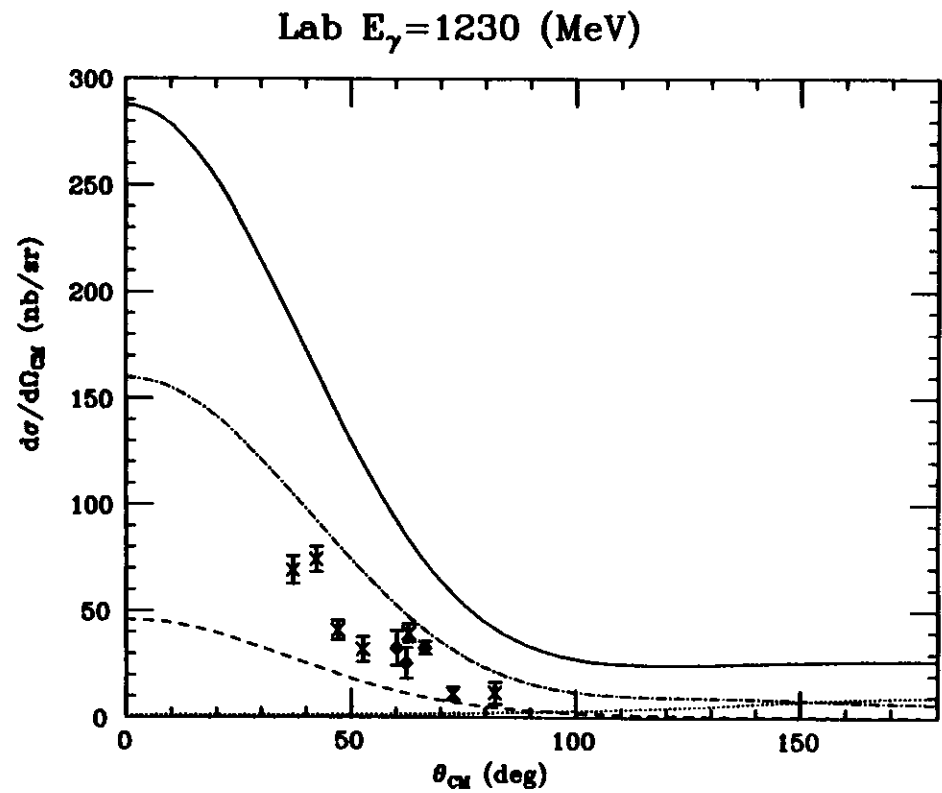


FIG. 4. CM frame differential cross section at $E_\gamma = 1230$ MeV. Legend for the calculation is as in Fig. 2; data are from Ref. [2] (X's), and Ref. [21] (diamonds).

Lab $E_\gamma = 1500$ (MeV)

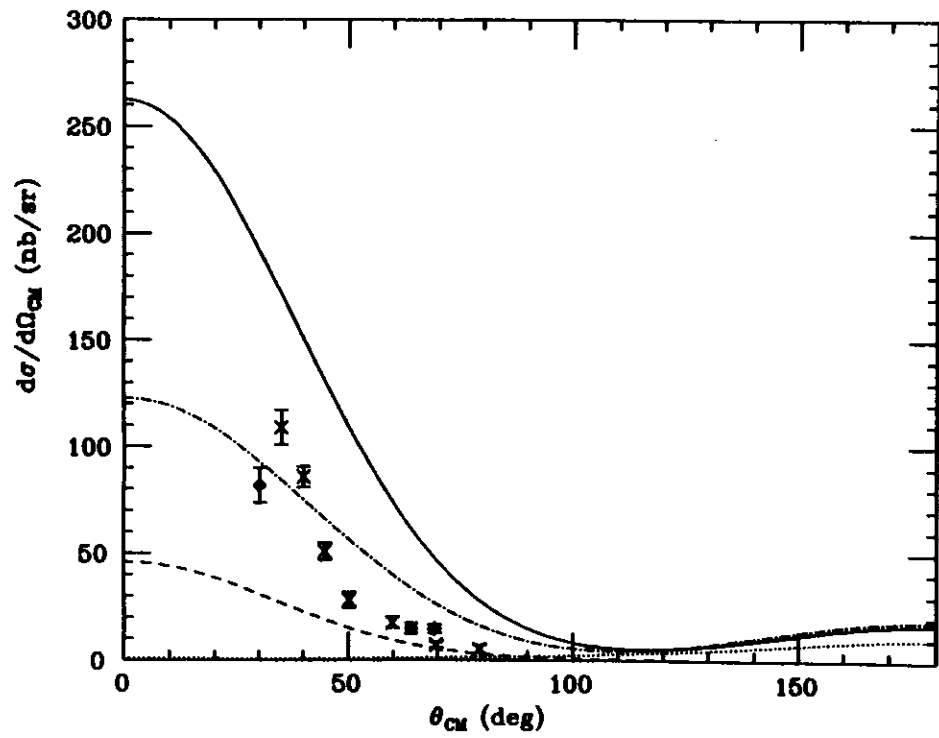


FIG. 5. CM frame differential cross section at $E_\gamma = 1500$ MeV. Legend as in Fig. 4.